RESEARCH ARTICLE

NANO · MICRO small
www.small-journal.com

Maximizing Porosity and Water Sorption in Covalent Organic Frameworks via β-Ketoenamine Linkages

Rasha G. AbdulHalim, Bikash Garai, Juul S. De Vos, Sander Borgmans, Lydia Gkoura, Sabu Varghese, Farah Benyettou, Mark A. Olson, Sven M. J. Rogge, and Ali Trabolsi**

Controlling the crystallinity and porosity of 2D covalent organic frameworks (2D COFs) is crucial for their applications in science and technology. Herein, the construction of 2D COFs, COF-TP-X, is reported using a multicomponent reaction strategy that introduces β-ketoenamine linkages into isostructural imine-linked COFs. This approach yields materials with exceptional crystallinity, stability, and tunable hydrophilicity. The integration of β-ketoenamine linkages promotes intralayer planarity via NH···O hydrogen bonds and enhances π-electronic conjugation within and between layers. By partially substituting (43 mol%) 1,3,5-triformylbenzene with 1,3,5-triformylphloroglucinol, an outstanding gravimetric surface area of 1,984 $m^2\ g^{-1}$ and a pore volume of 0.8 $cm^3\ g^{-1}$ are achieved—a remarkable two-fold increase compared to mono-linker counterparts. Moreover, COF-TP-X exhibits an exceptional water uptake capacity of 0.70 g g^{-1} (70 wt.%) and superior hydrolytic stability, as confirmed by over 200 cycles of water adsorption–desorption experiments. Furthermore, molecular simulations reveal the significant role of electrostatic interactions between β-ketoenamine linkages in enhancing interlayer stacking and crystallinity. The findings provide key insights into COF design via a mixed-linker strategy, representing a significant advancement in developing COFs with superior performance and paving the way for their industrial applications.

1. Introduction

In the ever-evolving landscape of materials science, porous materials have attracted considerable attention in science and technology. In particular, covalent organic frameworks (COFs) have emerged as a thriving class of functional solid-state materials characterized by lightweight elements linked by strong covalent bonds.[1]

COFs are rapidly gaining recognition for their transformative potential in various technological applications including water treatment,[2] energy storage,[3] catalysis,[4] optoelectronics,[3,5] and gas adsorption and separation.[6] The appeal of COFs for these applications stems from their inherent structural features, such as crystallinity, high surface area, pore volume, accessible pore system and modular nature.[1]

In 2D COFs, particularly imine-linked COFs, the process of structure formation begins with the precipitation of an amorphous polymer from solution followed by a transformation into a crystalline framework.[1,7] This transformation is facilitated by the dynamic reversibility of the imine within the precipitate.[1,8]

Furthermore, the covalent connectivity in the formed layers extends exclusively in 2D, which emphasizes the significant role that weak interactions[9] between the molecular layers play in achieving crystalline structures with accessible surface area and structural stability. Non-covalent interactions include both intramolecular

R. G. AbdulHalim, B. Garai, L. Gkoura, F. Benyettou, A. Trabolsi
Chemistry Program
New York University Abu Dhabi
Saadiyat Island 129188, UAE
E-mail: ali.trabolsi@nyu.edu

J. S. De Vos, S. Borgmans, S. M. J. Rogge
Center for Molecular Modeling
Ghent University
Technologiepark-Zwijnaarde 46, Zwijnaarde 9052, Belgium
E-mail: Sven.Rogge@ugent.be

The ORCID identification number(s) for the author(s) of this article can be found under https://doi.org/10.1002/smll.202508046

DOI: 10.1002/smll.202508046

S. Varghese
Core and Technology Platform
New York University Abu Dhabi
Saadiyat Island 129188, UAE

M. A. Olson
Department of Physical and Environmental Sciences
Texas A&M University-Corpus Christi
6300 Ocean Dr., Corpus Christi, TX 78412, USA

B. Garai, A. Trabolsi
Water Research Center
New York University Abu Dhabi
Saadiyat Island 129188, UAE

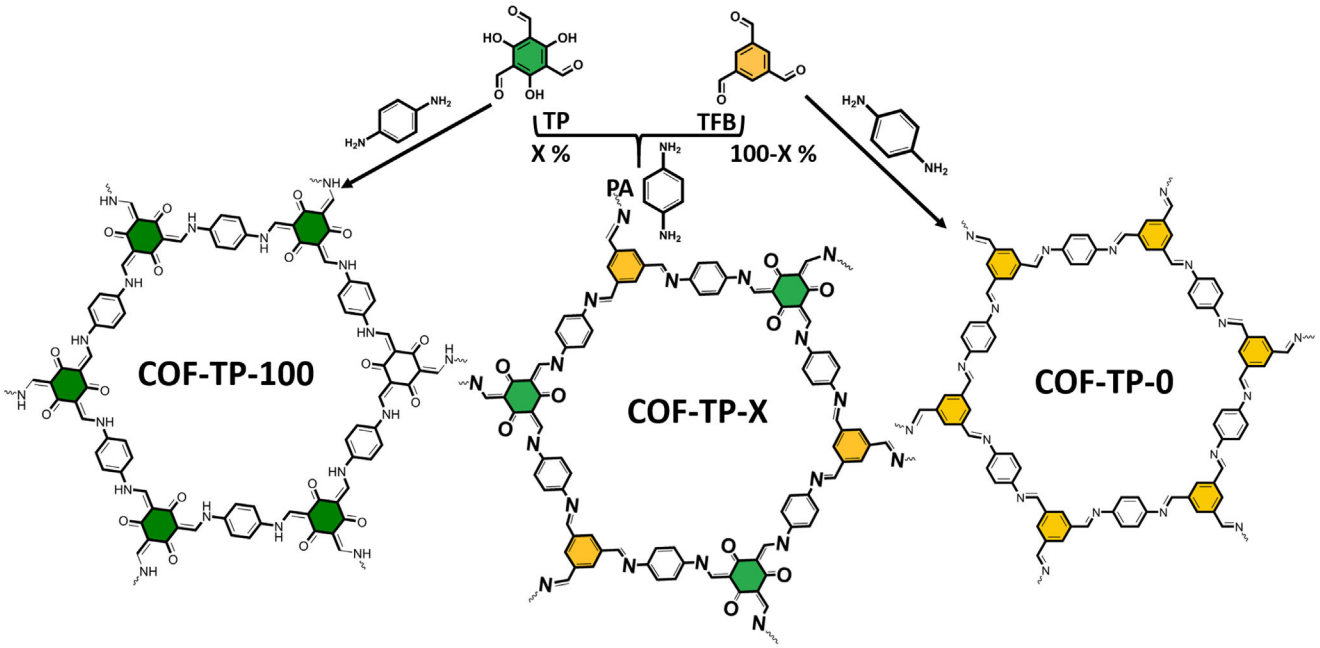

Figure 1. Schematic representation of the synthesis and structures of COF-TP-**100**, COF-TP-**0**, and COF-TP-**X** synthesized from a mixture of TP and TFB.

interactions, which serve to enhance the planarity of the layers for better alignment, and intermolecular interactions, which enhance π–π stacking.[10] The interactions between the extended π-systems are primarily responsible for promoting or inhibiting the stacking between the layers, consequently, influencing the overall crystallization of the network. For example, by introducing complementary forces into the neighboring layers of electron-rich and deficient layers, we can control the interactions between the layers of the formed COFs and thus their properties.[11]

The crystalline nature of COFs ensures well-defined porosity and unrestricted access to the active sites within the framework. These are indispensable properties for industrial applications such as catalysis, energy storage, and gas adsorption and separation.[12] To improve the crystallinity and porosity of the framework, it is imperative to consider and address the reversibility of the formed linkage and the interactions between the layers.

In searching for high-performance COFs, it is necessary to broaden the scope of applications of COFs by exploring and developing new linkages. This progress aims to turn them from being mere end products in a synthetic pathway into intermediates that can be transformed into otherwise inaccessible novel functional materials.

In this context, researchers have thoroughly investigated tuning variables such as linkages used and complementary interactions between the layers in order to improve the stability and inter-layer stacking. To date, various linkages, such as boronic acid and boronate ester formation trimerization,[8a,13] trimerization of nitriles,[14] and Schiff base reactions,[11,15] have been widely used and studied due to the availability, affordability, and enhanced stability of precursors to moisture and a wide pH range.[16]

To further elucidate the correlation between linkage formation and interlayer interactions, we adopted the multicomponent reaction approach (MCR) to increase the crystallinity and stability, and to control the hydrophilicity of the formed COFs by introducing β-ketoenamine linkages into isostructural imine-based COFs.

We report the synthesis of COFs with mixed linkers including β-ketoenamine and imine linkages through the condensation of primary amines and aldehydes. In this work, we present a criterion for overcoming the barriers that lead to COFs with remarkable crystallinity and porosity as the percentage of β-ketoenamine in the framework increases up to 50%. Furthermore, we illustrate the significant influence of β-ketoenamine on the chemical environment of COFs by tuning the hydrophilicity of the framework without compromising the overall water uptake capacity.

2. Results and Discussion

The condensation of *p*-phenylenediamine (PA) with either triformylbenzene (TFB) or triformylphloroglucinol (TP) forms the corresponding hexagonal 2D layered TFB-COF[15a] and TP-COF.[17] These COFs belong to the same space group forming extended hexagonal structures with slipped AA stacking of layers. This stacking with small, non-zero layer offsets is confirmed by the excellent agreement between the PXRD patterns in Figure 2d and the theoretical patterns predicted from *operando* molecular dynamics simulations in Figure S10 (Supporting Information).[18] Since both networks are prepared under identical reaction conditions, they provide an ideal platform to study the effect of mixing the two linkers in different ratios on the resulting COF structural properties.

To demonstrate this strategy, we opted for a three-component system in which we condensed a mixture of TFB and TP at different molar ratios with PA to form mixed linker COFs, referred to as COF-TP-**X** (**X** = [TP]/([TFB]+ [TP]) × 100).

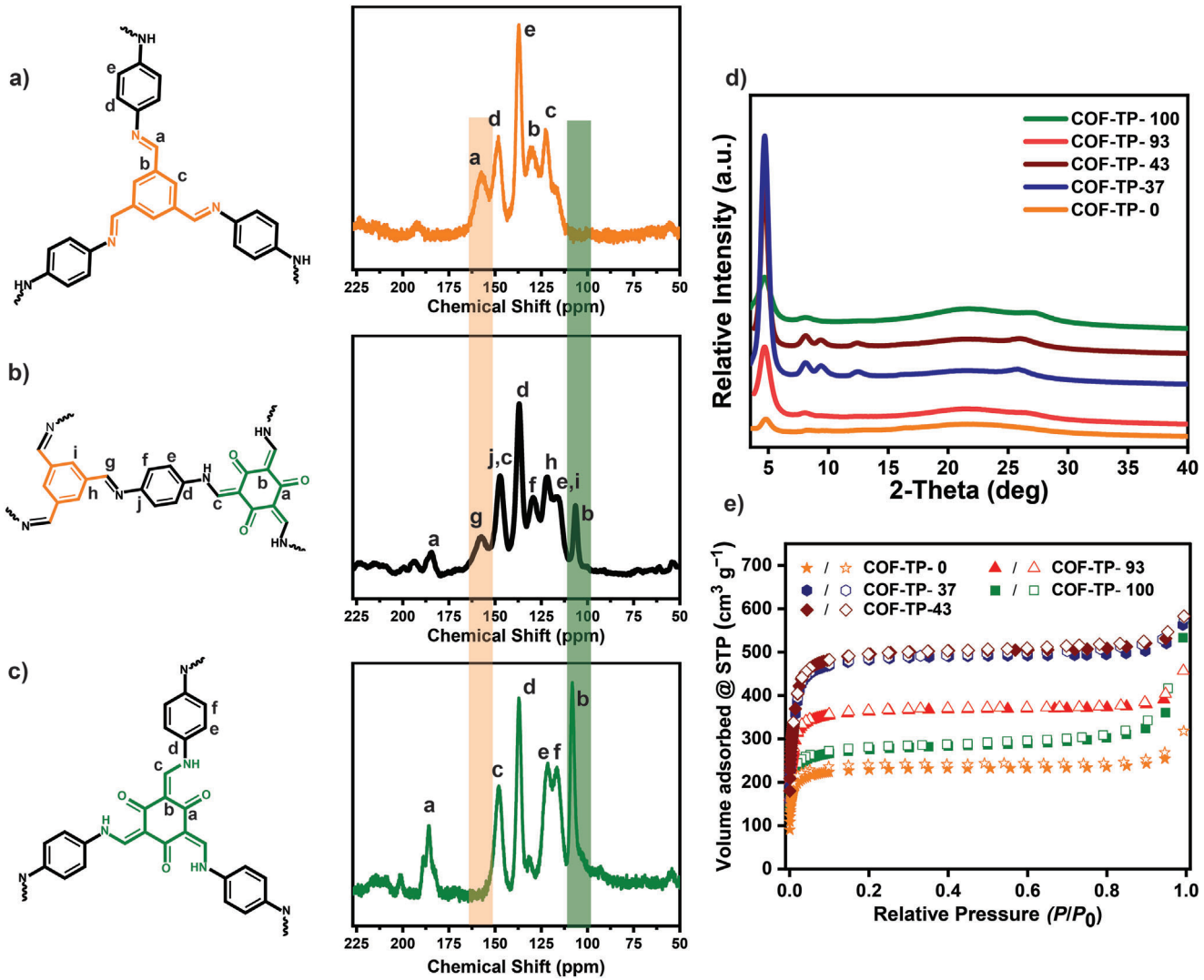

Figure 2. ^{13}C solid-state NMR spectra of (a) COF-TP-**0**, (b) mixed linker COF-TP-**X**, and (c) COF-TP-**100**. (d) PXRD patterns of COF-TP-**X**. (e) N_2 adsorption isotherms of COF-TP-**X**.

2.1. Structural Analysis and Characterization of COF-TP-X

The COF-TP-**X** structures were synthesized under the same conditions used for the formation of the mono-linker COFs (1.0:0.2 1,4-dioxane / acetic acid, 120 °C, 3 days). In our study, we prepared a total of five mixtures of TP/TFB by varying the mol.% of TP from 0% to 100%, while maintaining a molar ratio of PA to total aldehyde of 2:3 (**Figure 1**; Table S1, Supporting Information). Characterization of the activated materials by Fourier transform infrared (FTIR) spectroscopy provides direct evidence for the complete consumption of the starting materials, based on the absence of the N—H stretching bands of PA (3100–3300 cm^{-1}) and the carbonyl stretching bands of TP (1635 cm^{-1}) and TFB (1691 cm^{-1}). Simultaneously, new peaks appear at ≈1593 cm^{-1} indicating the formation of C═N (from the TFB linker) and ≈1577 cm^{-1} arising from the C═C stretching of the β-ketoenamine linkage (from the TP linker). We observe that the intensity of the peak associated with the C═C bond increases as the TP content increases, indicating the successful integration of the TP linker at different monomeric feeds (Figures S1 and S2, Supporting Information). As a result, isolation of COF-TP-**X** (**X** represents different mol.% of TP in COF) with a mixed imine and β-ketoenamine linkages was successfully isolated for COF-TP-**20/35/75**. This was further corroborated by ^{13}C cross-polarization/magic angle spinning (CP-MAS) solid NMR spectroscopy (**Figure 2a–c**; Figure S2, Supporting Information).

The ^{13}C CP-MAS spectra reveal comparable spectra for both mono-linker and the multicomponent COFs (COF-TP-**X**) with five peaks that can be assigned to the respective carbon atoms in the repeating unit. We observe a distinct peak at 107 ppm corresponding to the exocyclic sp^2-hybridized carbons C═C of the β-ketoenamine linkage, in addition to the characteristic imine carbon C = N of the TFB linker at 157 ppm. Furthermore, the broad peak at ≈184 ppm corresponds to the presence of ca groups (C═O) of the β-ketoenamine linkage, with all other carbon resonances located between 107 and 157 ppm.

As evident from the CP-MAS spectra of COF-TP-**0**, the peak at 157 ppm corresponding to the C═N linkages is absent in the spectrum of the mono-linker COF-TP-**100**. Additionally, the carbon signals of the C═C and C═O appear as intense peaks at 107 and 184 ppm, respectively, which are absent in COF-TP-**0**. To further support the complete linkage integration among the synthesized COF-TP-**X**, and to quantitatively determine the ratio of the two linkers, we used solid-state direct polarization ^{13}C MAS NMR spectroscopy (Figure S3, Supporting Information). The quantitative spectra were recorded with a recycle delay of 20 s.

The distinct peak at 107 ppm, corresponding to the exocyclic sp^2 hybridized carbons C═C of the TP linker, could be clearly integrated in all samples and compared with the imine C═N peak at 157 ppm. By integrating the resonance peak intensities, the TP content was found to be at 93% for COF-TP-**75**, at 43% for COF-TP-**35**, and at 37% for COF-TP-**20**. These carbon integrations quantitatively confirmed the lattice components of the formed COF-TP-**X**. The deviation from theoretical values indicates the different reaction kinetics of the two linkers, in which the β-ketoenamine forms at a faster rate than the imine linkage. As we confirm the mol.% of TP content in each of the formed COFs, we next highlight the porosity, chemical stability, and crystallinity of COF-TP-**93**, COF-TP-**43**, and COF-TP-**37** and compare them with the mono-linker COFs (TP content at 0% and 100%). The morphology of COF-TP-**X** structures was studied by scanning electron microscopy (SEM, Figure S4, Supporting Information) and transmission electron microscopy (TEM, Figure S4, Supporting Information).

To assess the permanent porosity of the isolated COF-TP-**X**, we conducted nitrogen (N_2) adsorption measurements at 77 K. The adsorption measurements revealed a fully reversible type-I isotherm, which is characteristic of microporous materials with permanent microporosity for COF-TP-**X** structures, (Figure 2e). COF-TP-**43** has the highest surface area (S_{BET}) of 1984 $m^2\ g^{-1}$ and pore volume of 0.8 $cm^3\ g^{-1}$, as shown in Table S2 (Supporting Information), followed by COF-TP-**37** and COF-TP-**93**, then COF-TP-**100** and COF-TP-**0**. Surface area is a quantitative parameter that is very sensitive to polymerization, crystallinity and activation conditions.[19] The high surface area indicates that the COFs are microporous materials with remarkable nitrogen uptake at low relative pressures. Since the mixed linkers have similar dimensions, we expected the surface area of the mixed-linker COFs to be within the range of the mono-linker COFs. Interestingly, as the mol.% of TP increases, both the measured surface area and pore volume reach optimal values with a 2-fold increase for COF-TP-**43** compared to the mono-linker COF-TP-**100** and COF-TP-**0**.

The larger surface area and pore volume, observed with increasing mol.% of TP in the COF-TP-**X** structures, reflect the crucial role of keto forms in facilitating intralayer planarity via NH···O hydrogen bonding and promoting electronic conjugation within the layer itself and between neighboring layers. Hence more ordered layers with accessible pore surfaces are formed. Figure S5A (Supporting Information), representing powder diffraction patterns of COF-TP-**X** collected on a single-crystal X-ray diffractometer, clearly demonstrates that mixed-linker COFs exhibit enhanced crystallinity compared to single-component counterparts. In particular, the distinctly enhanced (100) reflection and the clear presence of (210), (200) and (310) planes for COF-TP-**43** indicate a highly ordered, quasi-eclipsed stacking arrangement with limited linker/node defects, as reported by Lotsch et al.[20]

To gain a fundamental atomic-level understanding of the exceptionally large surface area of the mixed-linker COFs, molecular dynamics simulations under *operando* conditions are performed using ab initio derived flexible force fields (Section computational simulations, SI). By varying the TP content in the investigated molecular systems, our calculations show that the nonlinear behavior of the gravimetric pore characteristics originates from two competing density effects. On the one hand, the relatively heavy oxygen atoms of TP units and the additional hydrogen atom of the β-ketoenamine linkage increase the density of materials with a higher TP content. On the other hand, COFs with a higher amount of TFB building blocks have a higher density since their layers are more compressed, as explained below. Therefore, the mono-linker materials demonstrate a significantly higher density compared to the mixed-linker COFs (Figure S11, Supporting Information). Since the gravimetric surface area and pore volume inversely correlate with the density, these properties are maximized for the mixed-linker COFs compared with the mono-linker COFs. Within the computationally investigated COFs, the COF with a TP content of 40% exhibits the lowest density. Accordingly, the materials with a TP content between 20% and 40% show the highest surface area, and those with a TP content between 40% and 70% have the highest pore volume, as demonstrated in **Figure 3**. These predictions successfully reproduce the experimental trend qualitatively, although a full quantitative agreement could not be achieved, as explained in more details in the Supporting Information.

While the heavier TP units explain why COFs with a high TP content are denser, the opposite effect – densification of the structure for high TFB content – is more surprising. However, it can be fully rationalized based on the interlayer interactions. As illustrated in Figure S12 (Supporting Information), increasing the TFB content reduces the electronic hindrance resulting in a shorter interlayer distance. Indeed, for COFs with a low TFB content, strong electrostatic interactions between a TP building block in one layer with TP or TFB units in neighboring layers limit the offset between neighboring layers to values between 0.20 and 0.40 nm. This smaller layer offset implies a larger interlayer distance (of ≈0.32 nm) for COFs with a low TFB content to prevent large repulsive van der Waals interactions (Figure S13, Supporting Information). In contrast, for COFs with a sufficiently high TFB content, neighboring layers contain only TFB units, interlayer electronic interactions are weaker due to the lower partial charges on the TFB units (Figure S8, Supporting Information). As a result of the reduced electronic hindrance, the offset in COFs with high TFB content increases to ≈0.42 nm (Figures S12 and S13, Supporting Information), allowing for a reduced interlayer distance below 0.30 nm due to minimized van der Waals repulsion.

The thermal stability of COF-TP-**X** was evaluated using thermogravimetric analysis (TGA). All COFs showed high thermal stability, showing no significant loss up to 400 °C under N_2 atmosphere (Figure S14, Supporting Information). However, as TGA is less sensitive to changes in the COF's periodic structure, the COF-TP-**X** samples were activated at elevated temperatures of 180, 240, 280, 320, and 380 °C and kept under vacuum for 12

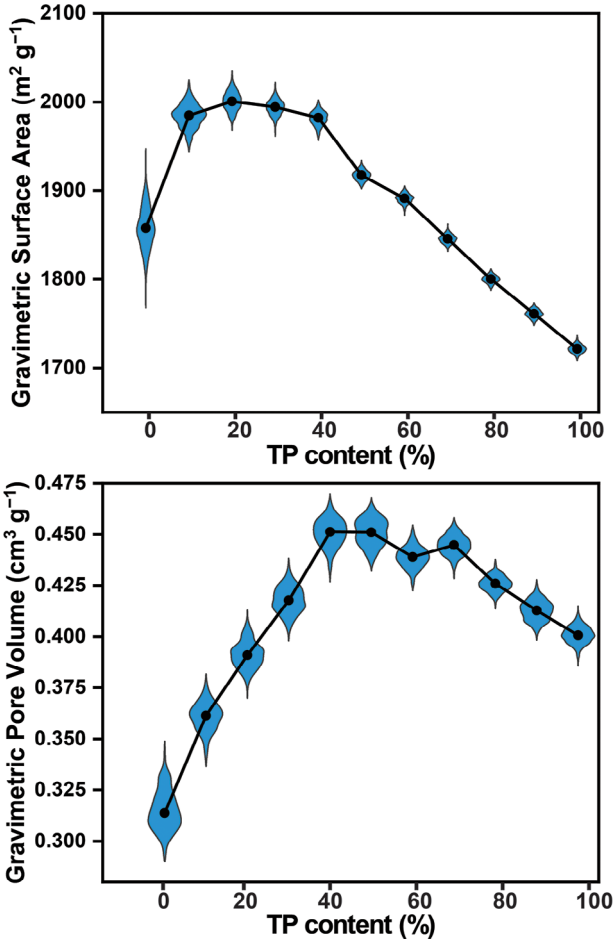

Figure 3. Dependency of the gravimetric surface area and pore volume on the TP content of various mixed-linker COFs, as predicted by molecular dynamics simulations at 77 K and 1 atm. The violin plots visualize the distribution during the simulation.

h. Then PXRD analysis and N_2 adsorption measurements were carried out to study the effect of heating on the crystallinity and porosity of the COF.

As can be seen in **Figures** 4 and S15 (Supporting Information), COF-TP-**X** retains type-I isotherms and maintains high structural stability when exposed to temperatures up to 380 °C. Remarkably, COF-TP-**43** maintained optimal porosity after heating to 240 °C, with a 16% loss in total surface area when heated to 380 °C. It is also noticeable that COF-TP-**X** samples retained long-range periodicity and structural identity at 380 °C (Figures S16 and S17, Supporting Information).

Given the distribution of ketoenamine moieties in the COF's skeleton, which reportedly confer high hydrolytic stability to the framework,[21] we aimed to assess and evaluate the water adsorption performance of COF-TP-**X** at different relative humidity (RH) levels by performing water adsorption measurements.

2.2. Water Adsorption Properties of COF-TP-X

The water vapor adsorption properties of COF-TP-**X** were investigated using the IGAsorp vapor sorption analyzer from Hiden

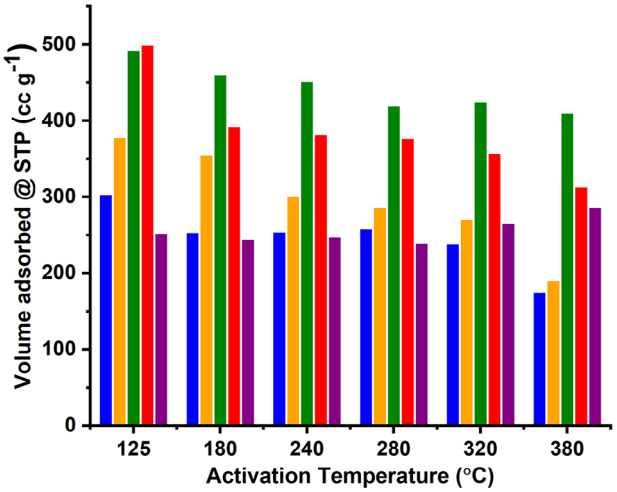

Figure 4. Effect of activation temperature (125, 180, 240, 280, 320 and 380 °C) on surface area of COF-TP-**0** (orange), COF-TP-**37** (blue), COF-TP-**43** (maroon), COF-TP-**93** (red) and COF-TP-**100** (green).

Isochema. The water vapor partial pressure was automatically controlled by mixing the wet vapor feed with a N_2 line so that N_2 serves as a carrier gas for the water vapor. The sample was pretreated by drying at 125 °C in the presence of N_2 drying carriers for 5 h. The "dry mass" of the sample was measured under N_2 at equilibrium (25 °C) before water vapor was gradually dosed into the chamber. The stability of each of the collected samples was verified by FT-IR and N_2 adsorption measurements after each run (Figures S18 and S19, Supporting Information). The adsorption isotherms obtained at equilibrium were measured between 0% RH and 98% RH at ambient temperature (25 °C), as shown in **Figure** 5. Before water adsorption measurements, acetone-exchanged samples were soaked in liquid water and their chemical stability was monitored with PXRD overo 24 h and one week (Figure S20, Supporting Information).

The water vapor adsorption isotherm of the fully activated COF-TP-**X** samples displays a type-V S-shaped (sigmoidal) in both adsorption and desorption branches. The onset pressure points depend on the mol.% of TP embedded in the framework. A higher concentration of the hydrophilic sites, the ketoenamine moieties, increases the hydrophilicity of the framework, resulting in an earlier onset of water uptake. Water molecules are initially adsorbed on the oxygen groups, forming bound water,[22] Figure 5 (top view). This is followed by the adsorption of more water molecules, intermediate water, as they form new hydrogen bonds with the bound water. Subsequently, these intermediate water molecules become nucleation sites for the formation of large water clusters at higher relative humidity, where both intermediate and free water molecules accumulate into the pores. This is evident in the hysteresis loop which becomes more pronounced in the samples with lower ketoenamine content as the framework becomes more hydrophobic and requires the formation of larger water clusters before capillary condensation occurs.[23]

COF-TP-**100** and COF-TP-**93** show water sorption isotherms with a steep pore-filling step at 20% RH (at 25 °C, Figure 5, dark turquoise and dark blue respectively) with a relatively small

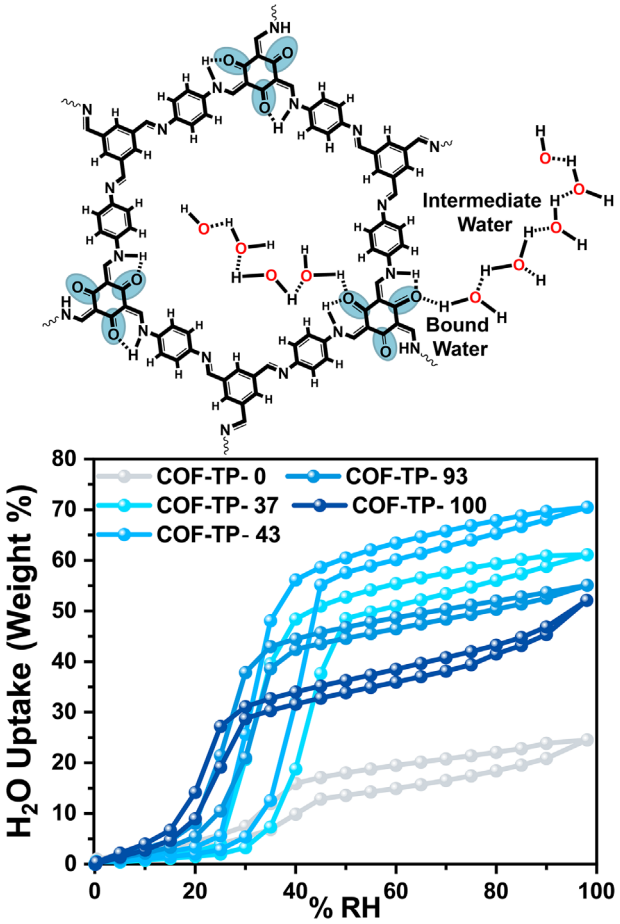

Figure 5. Top: schematic illustration of water interaction with hydrophilic sites. Bottom: Water adsorption isotherm of COF-TP-**X** (**X** = **0**, **37**, **43**, **94**, **100**), indicated by the color code.

hysteresis loop compared to other COFs.[24] The quick uptake reflects the capillary condensation of water molecules in the microporous 1D channels. While COF-TP-**100** reaches a saturation uptake value of 41 wt.% (648 $cm^3.g^{-1}$) at 80% RH followed by clusters agglomeration filling the interstitial spaces between microcrystallites.[25] COF-TP-**93** displays a total water adsorption capacity of 55 wt.% (685 $cm^3.g^{-1}$) at 98% RH, with the improved capacity being due to the enhanced surface area.

For COF-TP-**0**, COF-TP-**37**, and COF-TP-**43**, with lower ketoenamine content, we observe a delayed onset for all three frameworks starting at 30% RH. COF-TP-**43** exhibits an S-shaped water sorption isotherm with a pronounced hysteresis loop and a steep pore-filling step at 30% RH (Figure 5, turquoise curve). The maximal water uptake reaches 70 wt.% (877 $cm^3.g^{-1}$) at 98% RH, one of the highest among the microporous COFs.[24,26] COF-TP-**37** shows a similar behavior with a slightly less steep uptake, amounting to 61 wt.% (760 $cm^3.g^{-1}$) at 98% RH. The lower water uptake capacity is due to its lower porosity. In contrast, COF-TP-**0** shows a rather sluggish uptake between 30% and 45% RH with a total uptake capacity of 30 wt.% (403 $cm^3.g^{-1}$) at 90% RH.

To evaluate the recyclability and hydrolytic stability of the frameworks, each COF-TP-**X** was subjected to three cycles at equilibrium, followed by FT-IR, PXRD, and N_2 adsorption measurements. These COFs showed excellent recyclability as indicated by the almost identical water adsorption isotherms over three cycles as shown in Figure S21 (Supporting Information). The structural integrity of each of these COFs is preserved as shown by FT-IR (Figure S18, Supporting Information). However, COF-TP-**X** with low ketoenamine content (COF-TP-**0** and COF-TP-**37**) showed reduced crystallinity and porosity (Figure S19, Supporting Information) although COF-TP-**37** retains higher order and porosity compared to COF-TP-**0**.

On the other hand, COFs with higher ketoenamine content (COF-TP-**43**/ **93**/ **100**) show outstanding stability to water (Figure S19c–e, Supporting Information) with COF-TP-**43** showing the highest water uptake (70 wt.%) due to its higher porosity. Hence, COF-TP-**43** was selected for further water sorption studies starting by measuring the water sorption profiles at different temperatures (35, and 45 °C). As shown in Figure S24 (Supporting Information), similar behavior and isotherm shape to the sample collected at 25 °C was observed but with a relatively narrower gap and a slightly lower uptake.

Further cyclic measurements were conducted, between 20% and 85% RH, in order to evaluate the long-term water sorption performance of COF-TP-**43**, **Figure 6d**. Over 200 water vapor adsorption–desorption cycles were performed with COF-TP-**43** at room temperature and non-equilibrium conditions (Figure 6d; Figure S22, Supporting Information) with adsorption at 85% RH and desorption at 20% RH. COF-TP-**43** showed high and steady cyclic water vapor adsorption as it maintains a high-water uptake of 45 wt.%. The water adsorption isotherm as well as FT-IR and PXRD patterns (Figures S23,S26, and S27, Supporting Information) obtained on the extensively recycled sample confirm the hydrolytic stability of COF-TP-**43** and the retention of its structural features.

In light of the high stability of water, further experiments were conducted, under more practical conditions, to evaluate the effect of varying the relative humidity and temperature during adsorption and desorption on the performance of the material. We determined the optimal desorption temperature by saturating the material at 45%, 55% and 65% RH at 25 °C (Figure 6b) followed by desorption at 0% RH and temperatures of 35, 45 or 65 °C and (Figure 6c; Figure S25, Supporting Information). As shown in Figure 6b,c, the steepest uptake occurs at 65% RH, reaching saturation in less than 50 min, whereas desorption occurs very fast at 65 °C to trigger the release of 0.45 g g^{-1}, reflecting the weak interactions between water and the framework.

3. Conclusion

In summary, we have successfully synthesized and improved the performance of microporous 2D COFs by incorporating β-ketoenamine linkages using the MCR approach. By creating mixed-linker COFs that contain both imine and β-ketoenamine linkages at varying percentages, the resulting COF-TP-**37**/**43**/**93** exhibits significantly higher crystallinity and surface area than the corresponding mono-linker COFs (**X** = 0% or 100%). The combination of TP and TFB yields new

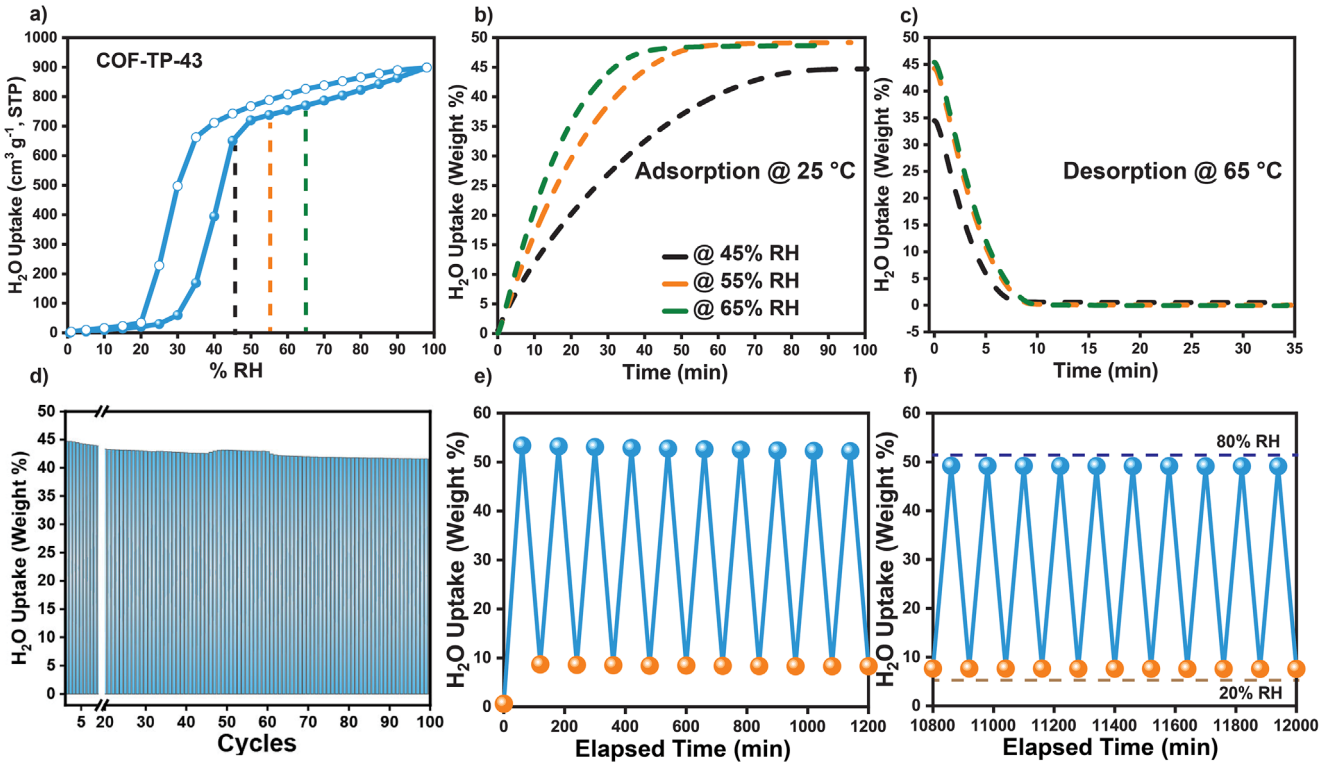

Figure 6. Water sorption properties of COF-TP-**43**. a) Water sorption at 25 °C. b) Dynamic vapor sorption properties: adsorption at 25 °C and 45, 55, and 65% RH. c) Desorption at 65 °C and 0% RH. d) Change of total mass variation of COF-TP-**43** during non-equilibrium adsorption and desorption over 100 cycles driven by continuous change in relative humidity between 20% RH and 85% RH at 25 °C. e,f) show the mass change between 20% RH and 85% RH of the first and last ten cycles respectively.

properties surpassing the linear combination of the individual components.

Molecular dynamics simulations indicate that the superior properties of mixed-linker COFs arise from two competing density effects. COFs with a higher proportion of TP units exhibit increased density; whereas COFs with only TFB units display higher density due to smaller interlayer distances. Both effects lead to reduced gravimetric properties in the mono-linker COFs. Additionally, strong electrostatic interactions between TP linkages in neighboring layers significantly influence the stacking behavior, which is not observed with layers containing only TFB linkages.

The mixed-linker COFs also demonstrate outstanding water sorption properties and thermal stability. Specifically, COF-TP-**43** shows a high-water uptake capacity of 70 wt.% and maintains exceptional long-term stability over more than 200 cycles of water adsorption-desorption experiments. Most importantly, COF-TP-**43** can adsorb up to 45 wt.% at 45–65% RH and desorb completely at 35–65 °C, underscoring its potential use in energy-efficient adaptive water harvesting devices.[27] Accordingly, COF-TP-**43** is a promising adsorbent currently under evaluation for such water harvesting devices.

Supporting Information

Supporting Information is available from the Wiley Online Library or from the author.

Acknowledgements

This work was supported by New York University Abu Dhabi and the NYUAD Water Research Center, funded by Tamkeen under the NYUAD Research Institute Award (project CG007). The research work was carried out using the Core Technology Platform (CTP) resources at NYUAD. J. S. D. V. acknowledges the Research Foundation Flanders (FWO) for a strategic basic (SB) research fellowship (grant no. 1S94521N). S. M. J. R. acknowledges funding by the Research Board of Ghent University (BOF, grant no. BOF/STA/202309/008) and the European Union (ERC-StG grant no. 101115787 – STRAINSWITCH). Views and opinions expressed are however those of the authors only and do not necessarily reflect those of the European Union or the European Research Council. Neither the European Union nor the granting authority can be held responsible for them. The computational resources (Stevin Supercomputer Infrastructure) and services used in this work were provided by the VSC (Flemish Supercomputer Center), funded by Ghent University, FWO, and the Flemish Government—department EWI.

Conflict of Interest

The authors declare no conflict of interest.

Data Availability Statement

The data that support the findings of this study are available on request from the corresponding author. The relevant computational input files and data are available on Zenodo at, https://doi.org/10.5281/zenodo.16733413.

Keywords

covalent organic framework, electrostatic interactions, multicomponent, layer stacking, water harvesting

Received: July 17, 2025
Revised: July 23, 2025
Published online:

[1] A. P. Côté, A. I. B., N. W. Ockwig, M. O'Keefe, A. J. Matzger, O. M. Yaghi, *Science* **2005**, *310*, 1166.
[2] W. Ji, L. Xiao, Y. Ling, C. Ching, M. Matsumoto, R. P. Bisbey, D. E. Helbling, W. R. Dichtel, *J. Am. Chem. Soc.* **2018**, *140*, 12677.
[3] S. Wan, F. Gándara, A. Asano, H. Furukawa, A. Saeki, S. K. Dey, L. Liao, M. W. Ambrogio, Y. Y. Botros, X. Duan, S. Seki, J. F. Stoddart, O. M. Yaghi, *Chem. Mater.* **2011**, *23*, 4094.
[4] a) X. Han, Q. Xia, J. Huang, Y. Liu, C. Tan, Y. Cui, *J. Am. Chem. Soc.* **2017**, *139*, 8693; b) Y. Li, W. Chen, R. Gao, Z. Zhao, T. Zhang, G. Xing, L. Chen, *Chem. Commun.* **2019**, *55*, 14538.
[5] a) J. M. Rotter, R. Guntermann, M. Auth, A. Mahringer, A. Sperlich, V. Dyakonov, D. D. Medina, T. Bein, *Chem. Sci.* **2020**, *11*, 12843; b) H. Wang, C. Qian, J. Liu, Y. Zeng, D. Wang, W. Zhou, L. Gu, H. Wu, G. Liu, Y. Zhao, *J. Am. Chem. Soc.* **2020**, *142*, 4862.
[6] a) H. Fan, A. Mundstock, A. Feldhoff, A. Knebel, J. Gu, H. Meng, J. Caro, *J. Am. Chem. Soc.* **2018**, *140*, 10094; b) X. Guan, H. Li, Y. Ma, M. Xue, Q. Fang, Y. Yan, V. Valtchev, S. Qiu, *Nat. Chem.* **2019**, *11*, 587; c) F. Jin, E. Lin, T. Wang, S. Geng, L. Hao, Q. Zhu, Z. Wang, Y. Chen, P. Cheng, Z. Zhang, *J. Am. Chem. Soc.* **2022**, *144*, 23081.
[7] Q. Gao, L. Bai, Y. Zeng, P. Wang, X. Zhang, R. Zou, Y. Zhao, *Chem. Eur. J.* **2015**, *21*, 16818.
[8] a) A. P. Cote, A. I. Benin, N. W. Ockwig, M. O'Keeffe, A. J. Matzger, O. M. Yaghi, *Science* **2005**, *310*, 1166; J. W. Colson, W. R. Dichtel, *Nat. Chem.* **2013**, *5*, 453.
[9] a) S. J. Lyle, P. J. Waller, O. M. Yaghi, *Trends Chem.* **2019**, *1*, 172; b) S. B. Alahakoon, G. T. McCandless, A. A. Karunathilake, C. M. Thompson, R. A. Smaldone, *Chem. Eur. J.* **2017**, *23*, 4255.
[10] N. Huang, P. Wang, D. Jiang, *Nat. Rev. Mater.* **2016**, *1*, 16068.
[11] X. Chen, M. Addicoat, S. Irle, A. Nagai, D. Jiang, *J. Am. Chem. Soc.* **2013**, *135*, 546.
[12] Y. Xie, T. Pan, Q. Lei, C. Chen, X. Dong, Y. Yuan, J. Shen, Y. Cai, C. Zhou, I. Pinnau, Y. Han, *Angew Chem Int. Ed. Engl.* **2021**, *60*, 22432.
[13] H. M. El-Kaderi, J. R. Hunt, J. L. Mendoza-Cortes, A. P. Cote, R. E. Taylor, M. O'Keeffe, O. M. Yaghi, *Science* **2007**, *316*, 268.
[14] a) V. S. Vyas, F. Haase, L. Stegbauer, G. Savasci, F. Podjaski, C. Ochsenfeld, B. V. Lotsch, *Nat. Commun.* **2015**, *6*, 8508; b) S. Y. Yu, J. Mahmood, H. J. Noh, J. M. Seo, S. M. Jung, S. H. Shin, Y. K. Im, I. Y. Jeon, J. B. Baek, *Angew Chem Int. Ed. Engl.* **2018**, *57*, 8438.
[15] a) S. Y. Ding, J. Gao, Q. Wang, Y. Zhang, W. G. Song, C. Y. Su, W. Wang, *J. Am. Chem. Soc.* **2011**, *133*, 19816; b) F. J. Uribe-Romo, J. R. Hunt, H. Furukawa, C. Klöck, M. O'Keeffe, O. M. Yaghi, *J. Am. Chem. Soc.* **2009**, *131*, 4570.
[16] L. Bourda, C. Krishnaraj, P. Van Der Voort, K. Van Hecke, *Mater. Adv.* **2021**, *2*, 2811.
[17] S. Kandambeth, A. Mallick, B. Lukose, M. V. Mane, T. Heine, R. Banerjee, *J. Am. Chem. Soc.* **2012**, *134*, 19524.
[18] S. Borgmans, S. M. J. Rogge, J. S. De Vos, C. V. Stevens, P. Van Der Voort, V. Van Speybroeck, *Angew Chem Int. Ed. Engl.* **2021**, *60*, 8913.
[19] E. Vitaku, W. R. Dichtel, *J. Am. Chem. Soc.* **2017**, *139*, 12911.
[20] S. Van Gele, S. Bette, B. V. Lotsch, *JACS Au* **2025**, *5*, 388.
[21] a) S. Chandra, D. Roy Chowdhury, M. Addicoat, T. Heine, A. Paul, R. Banerjee, *Chem. Mater.* **2017**, *29*, 2074; b) L. M. Lanni, R. W. Tilford, M. Bharathy, J. J. Lavigne, *J. Am. Chem. Soc.* **2011**, *133*, 13975; c) Y. Zhang, X. Shen, X. Feng, H. Xia, Y. Mu, X. Liu, *Chem. Commun.* **2016**, *52*, 11088.
[22] H. Lu, W. Shi, J. H. Zhang, A. C. Chen, W. Guan, C. Lei, J. R. Greer, S. V. Boriskina, G. Yu, *Adv. Mater.* **2022**, *34*, 2205344.
[23] E.-P. Ng, S. Mintova, *Microporous Mesoporous Mater.* **2008**, *114*, 1.
[24] B. P. Biswal, S. Kandambeth, S. Chandra, D. B. Shinde, S. Bera, S. Karak, B. Garai, U. K. Kharul, R. Banerjee, *J. Mater. Chem. A* **2015**, *3*, 23664.
[25] L. Liu, S. J. Tan, T. Horikawa, D. D. Do, D. Nicholson, J. Liu, *Adv. Colloid Interface Sci.* **2017**, *250*, 64.
[26] a) L. H. Chen, W. K. Han, X. Yan, J. Zhang, Y. Jiang, Z. G. Gu, *ChemSusChem* **2022**, *15*, 202201824; b) C. Sun, Y. Zhu, P. Shao, L. Chen, X. Huang, S. Zhao, D. Ma, X. Jing, B. Wang, X. Feng, *Angew Chem. Int. Ed. Engl.* **2023**, *62*, 202217103; c) L. Stegbauer, M. W. Hahn, A. Jentys, G. Savasci, C. Ochsenfeld, J. A. Lercher, B. V. Lotsch, *Chem. Mater.* **2015**, *27*, 7874.
[27] H. A. Almassad, R. I. Abaza, L. Siwwan, B. Al-Maythalony, K. E. Cordova, *Nat. Commun.* **2022**, *13*, 4873.